Twin-Image-Free Holography: A Compressive Sensing Approach

Wenhui Zhang,[1,2] Liangcai Cao,[1,*] David J. Brady,[2,†] Hua Zhang,[1,2] Ji Cang,[1] Hao Zhang,[1] and Guofan Jin[1]
[1]State Key Laboratory of Precision Measurement Technology and Instruments, Department of Precision Instruments, Tsinghua University, Beijing 100084, China
[2]Department of Electrical and Computer Engineering, Box 90291, Duke University, Durham, North Carolina 27708, USA

(Received 17 April 2018; published 30 August 2018)

Holographic reconstruction is troubled by the phase-conjugate wave front arising from Hermitian symmetry of the complex field. The so-called twin image obfuscates the reconstruction in solving the inverse problem. Here we quantitatively reveal how and how much the twin image affects the reconstruction and propose a compressive sensing (CS) approach to reconstruct a hologram completely free from the twin image. Using the canonical basis, the incoherence condition of CS is naturally satisfied by the Fourier transformation associated with wave propagation. With the propagation kernel function related to the distance, the object wave diffracts into a sharp pattern while the phase-conjugate wave diffracts into a diffuse pattern. An iterative algorithm using a total variation sparsity constraint could filter out the diffuse conjugated signal and overcome the inherent physical symmetry of holographic reconstruction. The feasibility is verified by simulation and experimental results, as well as a comparative study to an existing phase retrieval method.

DOI: 10.1103/PhysRevLett.121.093902

Holography "freezes" the object wave front to realize lens-free imaging by interference [1]. The capability to record the phase makes holography widely used in both materials science and biomedicine as a means of quantitative phase imaging [2–4]. Through introducing a reference wave, the phase of the object wave is encoded into a hologram. As an interference technique, holography has the beauty of directly delivering the phase information and capturing three-dimensional information at just one exposure. However, the twin image caused by interference ultimately obfuscates the reconstruction [5].

To illustrate the twin image problem, a basic holography setup is shown in Fig. 1. The wave diffracted by a point is used as an object wave $U(x,y)$ and the nonscattered wave is used as a reference wave $R(x,y)$. Hologram H is at physics symmetry associated with the interference $H = |U(x,y)+R(x,y)|^2 = U^*(x,y)R(x,y) + U(x,y)R^*(x,y) + |U(x,y)|^2 + |R(x,y)|^2$, where the physical conjugation terms $U(x,y)R^*(x,y)$ and $U^*(x,y)R(x,y)$ are recorded. The original intention of holography was to record the wave front $U(x,y)$. Because the image sensor only responds to the light intensity, the conjugation wave $U^*(x,y)$, as a by-product, is also recorded. When the hologram is activated by the reconstruction wave, the "frozen" wave front would propagate to form the original object. The phase-conjugate wave front would also be activated and propagate. Reconstruction at the virtual image plane is the superposition of the original object and the twin image, as shown in Fig. 1(b). The conjugated situation appears at the real image plane. This is because hologram reconstruction is considered as a wave rather than as a transmittance reconstruction problem. For emission electron, x-ray, and gamma-ray holography [6,7], the twin image problem is especially pronounced because the distance between the source and the object is so small that the twin and original images are difficult to distinguish.

Twin images could be removed by experimental means in some particular instances [8–11]. The most common approaches use either off-axis [9] or phase-shifting strategies [11] to eliminate the twin image. Compared to these two approaches, in-line holography achieves high space bandwidth utilization and single-shot imaging with high stability. In visible light holography, lenses are usually introduced into the recording and reconstruction schemes to solve the twin image problem [10]. However, lenses would be less effective in the x-ray and gamma-ray holography. In electron emission holography, there is very limited space for lenses because the source needs to be placed close to the object. As a lens-free technique, in-line holography has the advantage of phase sensitivity, which is the optimal choice of some methods, such as coherent low energy electrons [12]. Recording a set of holograms at different wavelengths is a widely used approach [13,14]. In this way, the twin image is not removed, but suppressed, and this method is complicated to implement experimentally. In past decades, numerical methods [15–20] have emerged to eliminate the twin image. The most common employed numerical approach is phase retrieval (PR), which is a double-side constraint iteration. It requires a certain object's surrounding so-called support, which limits the reconstructed area. Recently, a deep learning-based approach using a neural network [21] was proposed for hologram reconstruction and proven effective. As a data-driven approach, massive data are needed as input to train

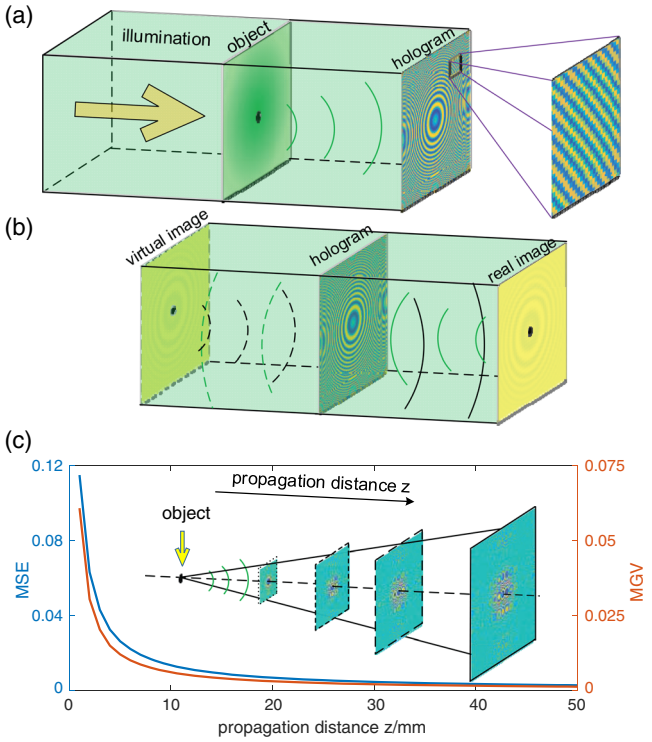

FIG. 1. Origin of the twin image and its influence to reconstructions. (a) Setup for inline Fresnel holography. The scattered object wave interferes with the unscattered reference wave forming inline hologram, which contains lots of "local gratings." (b) Both the virtual and real image plane would be a superposition of an in-focus image and an out-of-focus image due to the wave front propagation during reconstruction. Generally, the twin image appears as an out-of-focus image at the virtual image plane, which seriously blurs the reconstruction. (c) Twin image will have more of an effect on the reconstruction with decreased propagating distance under the evaluation of MSE and MGV.

the network for specific tasks. During training, the network is regarded as a black box without physical modeling of wave interference, which is, on the contrast, statistically inferred through data.

In this Letter, after physical modeling to the wave propagation via Fourier analysis and discovering the sparsity difference, we propose a physics-driven compressive sensing (CS) approach that imposes sparsity constraint. There is a significant difference between the reconstructed object and the twin image when they are sparsely expressed. The in-focus object has sharp edges while the out-of-focus twin image is diffuse. Eliminating the twin image with the sparsity difference is exactly where the superiority of the CS approach lies. The Fourier transformation to the signal via wave propagation and the used canonical basis naturally satisfy the incoherence condition and successfully combine holographic optics and CS. Further, CS has the inherent capacity to reduce noise in real situations. CS, as a powerful mathematical tool, has been proposed as a signal recovery approach based on sparsity constraints [22] and has been employed in diverse physical fields with significant breakthroughs, such as faster STORM [23], quantum state tomography [24], efficient measurement of quantum dynamics [25], predicting catastrophes in nonlinear dynamical systems [26], and simultaneous measurement of complementary observables [27]. In this Letter, we propose to remove the twin image by the CS approach based on the inherent symmetry physics of holography and the total variation sparsity constraint, which are the nature of holography and objects.

In Fig. 1(a), the scattered field $U(x,y)$ can be defined as

$$U(x,y) = \iint_{x,y\in\Sigma} \rho(x_1,y_1)h(x-x_1,y-y_1)dx_1dy_1, \quad (1)$$

where $\rho(x_1,y_1)$ represents the object density and h is the inverse Fourier transform of the propagation transfer function $\exp(ikz\sqrt{1-(\lambda f_x)^2-(\lambda f_y)^2})$ [28], [29] Eq. (3–74), and Σ represents the aperture function. While not only $U(x,y)$ but also its conjugation $U^*(x,y)$ is recorded. To make the reconstruction free from the twin image, it is essential to separate the signal point spread function (SPSF) and the twin image point spread function (TPSF), which is caused by the propagation of the phase-conjugate wave front $U^*(x,y)$, as shown in Fig. 1(b).

To mathematically describe this process, the Fourier analysis of wave front propagation is employed. From the Fourier transformation of Eq. (1), the bandwidth-limited angular spectrum of the scattered object wave front is $\tilde{U}(f_x,f_y) = \tilde{\rho}(f_x,f_y)\exp(ikz\sqrt{1-(\lambda f_x)^2-(\lambda f_y)^2}) \times P(f_x,f_y)$. $P(f_x,f_y)$ is unity when the frequency component is in the passband and zero otherwise. Assuming the input is real (similar analysis for imaginary), the angular spectrum of conjugated term can be obtained by the Fourier theorem as $\tilde{U}^*(-f_x,-f_y) = \tilde{\rho}(f_x,f_y) \times \exp(-ikz\sqrt{1-(\lambda f_x)^2-(\lambda f_y)^2})P(f_x,f_y)$ (see Supplemental Material for the derivation process [30]). The angular spectrum of the scattered object wave front and its conjugation have a pair of conjugated additional phases. During reconstruction, the phase $\exp(-ikz\sqrt{1-(\lambda f_x)^2-(\lambda f_y)^2})$ is multiplied to these two angular spectrums when backpropagating to the original object plane. The transfer functions of the reconstructed signal S and the twin image T can be readily determined from the object O with such a closed loop, which are $O \to S$:$P(f_x,f_y)$ and $O \to T$: $\exp(-2ikz\sqrt{1-(\lambda f_x)^2-(\lambda f_y)^2})P(f_x,f_y)$. Inverse Fourier transformation of these two transfer functions are SPSF and TPSF, respectively. SPSF denotes the inherent bandwidth-limited imaging feature, while TPSF denotes a bandwidth-limited double-diffraction process

that generates a nonsparse diffuse pattern. With decreased propagating distance, the twin image will have more of an effect on the reconstruction, as shown in Fig. 1(c), under the evaluation of mean square error (MSE) and mean gradient value (MGV) (see the Supplemental Material [30]).

Based on the Fourier analysis, a model associated with the CS framework was employed for the twin image removal. The unscattered field is assumed to be one without loss of generality and can be removed. Next, we need to processes $U^*(x,y)+U(x,y)+|U(x,y)|^2=2\mathrm{Re}\{U(x,y)\}+e(x,y)$. The square item $|U(x,y)|^2$ is considered the model error and rewritten as $e(x,y)$. Mapping from the diffracted wave field $U(x,y)$ to the preprocessed hologram $\tilde{H}$ can be expressed as $\tilde{H}=2\mathrm{Re}\{U(x,y)\}+e(x,y)$. If G represents the transform from $\rho(x_1,y_1)$ to $U(x,y)$, as illustrated in Eq. (1), then the complete mapping from the object density to the preprocessed hologram can be expressed as

$$\tilde{H}=2\mathrm{Re}\{G\rho\}+e. \tag{2}$$

Solving ρ with known $\tilde{H}$ and forward transform G is a typical inverse problem. Because of the conjugated symmetry of holography, both the original object and the twin image can be the solution of this inverse problem. The difference between them is the sparsity, while CS is one of the powerful methods that works based on sparsity constraint [22,31].

Based on the physical modeling via Fourier analysis, the forward model in Eq. (1) can be regarded as the combination of Fourier transformation as the measurement matrix G and an identity matrix (i.e., canonical basis) as the transformation matrix Ψ in the framework of CS, where the incoherence condition is naturally satisfied [22]. The physics behind the incoherence condition is that the measurement should be stable and the product of G and Ψ should be dense. Fortunately, the free-space wave propagation playing the role of Fourier transformation is a stable measurement means. In this case, the coherence parameter is equal to one, which is defined as

$$\mu_1(G,\Psi)=\sqrt{N}\max|\langle g_m,\psi_n\rangle|_{1\le m\le M,1\le n\le N}, \tag{3}$$

where g_m and ψ_n denotes the mth row of G and the nth column of Ψ, respectively. M and N are the dimensions of the matrixes.

Further, the forward model can be inverted by decompressive inference by either selecting a basis on which ρ is sparse or by enforcing a sparsity constraint on the total variation [32] of ρ. Since the sparsity difference is significant with total variation, the second approach is used and an algorithm based on two-step iterative shrinkage/thresholding is developed to address this inverse problem by minimizing this objective function,

$$\hat{\rho}=\arg\min_{\rho}\left\{\frac{1}{2}\|\tilde{H}-K\rho\|_2^2+\tau\|\rho\|_{TV}\right\}, \tag{4}$$

where K is the combined operator of forward transform G and taking the real part of the complex field. τ is the relative weight between l_2-norm of the residual, used to guarantee the estimation accuracy, and TV norm of the estimation, used as the function of sparsity. $\|\rho\|_{TV}=\sum_i\sqrt{|\Delta_i^x\rho|^2+|\Delta_i^y\rho|^2}$, where Δ_i^x and Δ_i^y denote the horizontal and vertical first-order local difference operations, respectively [33]. Generally, the more edges caused by the twin image, the larger the TV norm. The flow chart of the algorithm is shown in Fig. 2. After obtaining initialization ρ_0 by backpropagation from the normalized hologram and ρ_1 by denoising, the two-step iteration starts, where α and β are iteration coefficients. For each step, the residual would be calculated to guarantee monotonically decreasing with the iterative shrinkage/thresholding (IST) optimization [33]. The iterations will repeat until the residual is less than a threshold or a fixed loop number is finished, which could realize a twin-image-free reconstruction.

Both the twin image and the square item $e(x,y)$ could be removed with this algorithm by determining how much of the estimation should be placed at the object plane based on the correlation between the measurement hologram and the diffraction pattern that the estimation would produce. The square item e is inclined to cause the diffraction patterns, which have little correlation with the measurement hologram. Meanwhile, the diffraction pattern caused by the square item e is not sparse. Hence, most of the estimation error caused by e would be eliminated. For the twin image term, it is removed by the TV norm. As with the spatial frequency filter for twin elimination proposed by Leith and Upatnieks [9], the TV norm performs as a sparse filter to suppress the diffuse twin image. The corresponding code can be found in [34].

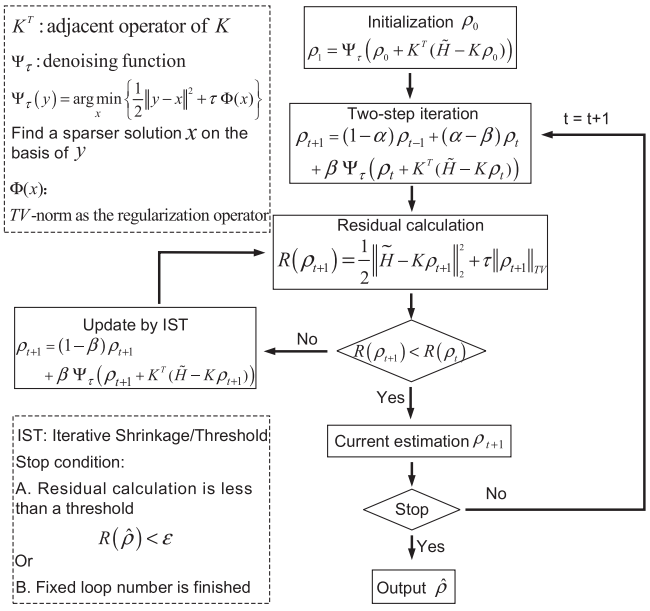

FIG. 2. Flow chart of the CS algorithm.

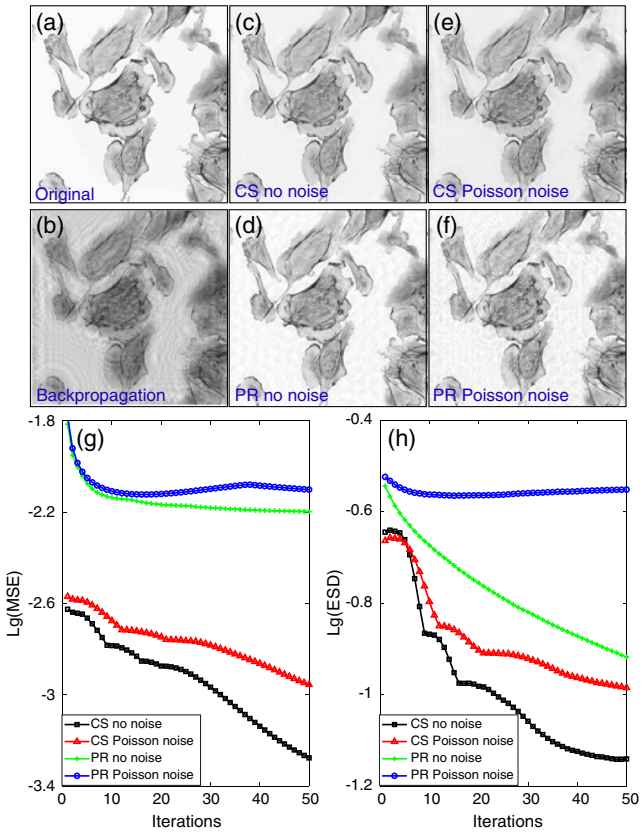

FIG. 3. Cell image and reconstructions. (a) Original image. (b) Backpropagation reconstruction with twin image. (c),(d) Reconstructions by CS and PR from a noise-free hologram after 50 iterations. (e),(f) Reconstructions by CS and PR from a Poisson noised hologram after 50 iterations. (g),(h) The curves of lg (MSE) and lg(ESD) changing with iteration.

Feasibility of the CS approach is verified both by simulated and experimental holograms. A comparison with a generalized PR algorithm used in [17] is carried out. Figure 3(a) shows a cell image used as amplitude object in simulation and Fig. 3(b) shows the traditional backpropagation reconstruction. Figures 3(c) and 3(d) show the reconstructions by CS and PR from a noise-free hologram, respectively. The CS reconstruction and the PR reconstruction from a Poisson noised hologram are shown in Figs. 3(e) and 3(f), respectively. These results are obtained after 50 iterations (results after 100 iterations can be found in the Supplemental Material [30]).

The performance of CS is better than PR, as shown in Fig. 3. To quantitatively illustrate the superiority of the CS approach, MSE [defined as $E = (1/M \times N)\sum_{i,j}|p(i,j) - p_0(x,y)|^2$, where $p(i,j)$ is the estimation distribution and $p_0(x,y)$ is the initial distribution] and the edge sparsity difference (ESD, the difference between the edge matrix of the reconstruction and that of the original object. Inspired by the sparsity criteria in autofocus algorithms [35]. See the Supplemental Material) of the reconstructions are calculated as evaluations. The smaller the value, the better the reconstruction. The curves of lg(MSE) and lg (ESD) changing with iterations are shown in Figs. 3(g) and 3(h), respectively. Either with or without noises, the MSE and ESD of CS are smaller than those of PR.

To further evaluate the robustness of the CS approach, white Gaussian noises under different signal to noise ratio (SNR = 10, 15, and 20 dB) are added to the particle hologram. The original particle image and its edge matrix image are shown in Fig. 4(a), as ground truth. The CS reconstruction and the PR reconstruction after 50 iterations are shown in Figs. 4(b)–4(d) and Figs. 4(e)–4(g), respectively. All the edge matrix images are calculated under the same threshold by the Sobel operator. Figure 4(h) shows the cross section of Figs. 4(d) and 4(g), which shows clearly CS has better performance than PR.

Through comparing the reconstructions under the same SNR, CS performs better over PR in which the edges are submerged by noise. The MSE of CS and PR is at a considerable level, while CS has a better ESD performance. Through comparing the reconstructions under different SNR, CS has a greater noise tolerance. It is beneficial to the inherent denoising capacity of CS, which finds sparse solution to the optimization problem, and the correlation evaluation in the model, which suppresses the noise not from diffraction. ESD shows clearly that the twin image is almost removed by CS even with noise. We tested two more images under different SNR levels, and CS also performed well (see the Supplemental Material [30]).

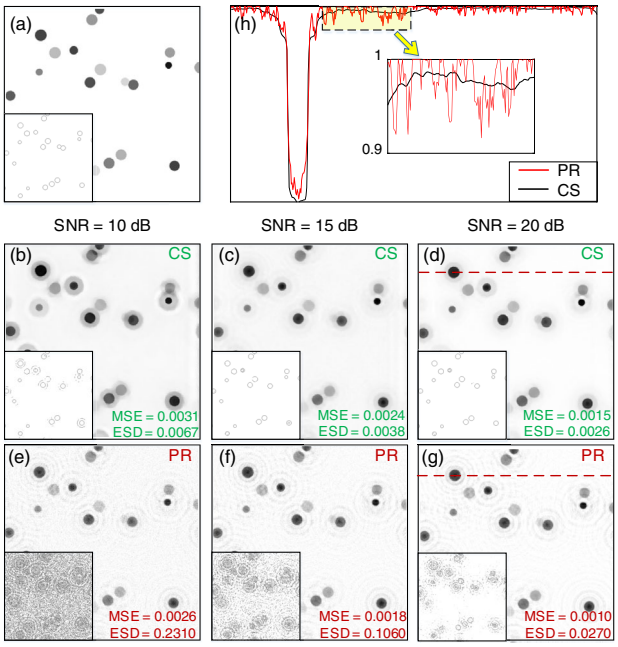

FIG. 4. Particle image and reconstructions under different SNR cases. (a) Original image and edge matrix image. (b)–(d) CS reconstructions after 50 iterations and corresponding edge matrix images. (e)–(g) PR reconstructions after 50 iterations and corresponding edge matrix images. (h) Cross section of (d) and (g).

As for the computation time, it takes about 35 s with a laptop (2.9 GHz CPU and 32 GB RAM) for 50 iterations with a 500×500 image. Besides, we proposed a blockwise method for the CS reconstruction, which could reduce the computation time greatly [36].

In the optical experiments, a plane wave at the wavelength of 532 nm is used for illumination. A resolution target is placed into the plane beam and controlled by a xyz stage. The distance between the target and the image sensor, which is a complementary metal oxide semiconductor with pixel pitch of 3.8 μm, is adjusted approximately to 9 mm to realize nearly on-chip holographic imaging. The captured hologram is shown in Fig. 5(a).

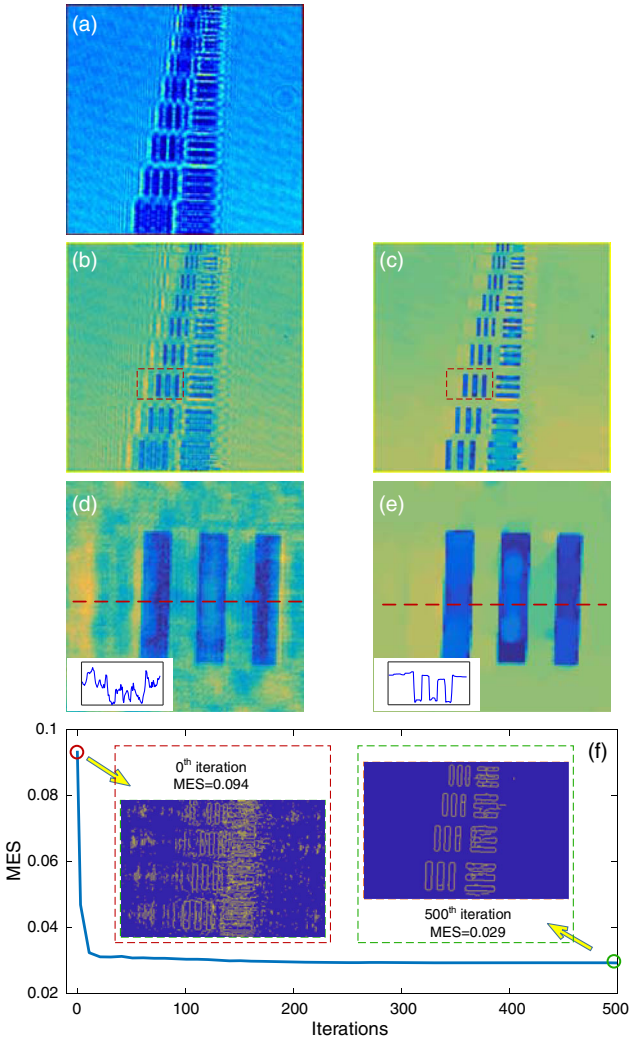

FIG. 5. Experimental hologram and reconstructions. (a) Captured hologram. (b) Conventional backpropagation reconstruction with twin image. (c) Estimation after 500 iterations by the CS approach without twin image. (d),(e) Enlarged area from (b) and (c), respectively. Intensity distributions along red lines in (d) and (e) show that the twin image is almost eliminated. (f) The curve of MES decreasing with iterations denotes that the twin image has been removed, which can be also observed through comparing the two subimages.

Because of the close distance between the target and the sensor plane, the twin image affects the reconstruction seriously, as shown in Fig. 5(b), while the twin image is almost removed after 500 iterations by the proposed CS approach, as shown in Fig. 5(c). To further quantify the twin image removal effect, a cross section of the zoomed area in Figs. 5(b) and 5(c) are drawn in Figs. 5(d) and 5(e).

Note that the reconstruction is smoother than the conventional reconstruction, which shows more twin image and blur defects. The mean edge sparsity (MES, calculated by the Sobel operator; see the Supplemental Material [30]) of the reconstructions is calculated and its curve is shown in Fig. 5(f). The less the edge amounts, the smaller the MES. The numerous messy boundaries caused by the twin image as shown in Fig. 5(f) are removed after iterations, while the desired signal boundaries remain.

In summary, a physics-driven CS approach is proposed to achieve twin-image-free holography. The physical symmetry of holography causes a sparsity difference between the reconstructed object image and twin image. This sparsity difference is exactly what CS needs for eliminating the twin image. With the used canonical basis, Fourier transform characteristics of wave propagation naturally satisfy the incoherence condition of CS. Employing compressive sensing to eliminate the twin image in holography is self-consistent and has been proved effective, powerful, and tolerant to noise, which is beneficial from the inherent denoising capacity of CS. This approach could be applied without limitations for electromagnetic wavelength, wave front shape, or support constraints. With a single hologram, the object can be retrieved by the total variation sparsity constraint, which is suitable for most of the natural objects.

This work was supported by the National Science Foundation of China (No. 61327902) and China Scholarship Council (201706210291).

*Corresponding author.
clc@tsinghua.edu.cn
†Corresponding author.
david.brady@duke.edu

[1] D. Gabor, Nature (London) **161**, 777 (1948).
[2] G. Popescu, *Quantitative Phase Imaging of Cells and Tissues*, (McGraw-Hill, New York, 2011).
[3] G. Popescu, T. Ikeda, K. Goda, C. A. Best, M. Laposata, S. Manley, R. R. Dasari, K. Badizadegan, and M. S. Feld, Phys. Rev. Lett. **97**, 218101 (2006).
[4] J. Nadeau, Y. Park, and G. Popescu, Methods **136**, 1 (2018).
[5] S. Ulf and P. O. J. Werner, Meas. Sci. Technol. **13**, R85 (2002).
[6] M. Tegze and G. Faigel, Nature (London) **380**, 49 (1996).
[7] P. Korecki and J. Korecki, Hyperfine Interact. **144**, 85 (2002).
[8] W. L. Bragg and G. L. Rogers, Nature (London) **167**, 190 (1951).

[9] E. N. Leith and J. Upatnieks, J. Opt. Soc. Am. **53**, 1377 (1963).
[10] O. Bryngdahl and A. Lohmann, J. Opt. Soc. Am. **58**, 620 (1968).
[11] I. Yamaguchi and T. Zhang, Opt. Lett. **22**, 1268 (1997).
[12] H.-W. Fink, H. Schmid, E. Ermantraut, and T. Schulz, J. Opt. Soc. Am. A **14**, 2168 (1997).
[13] S. Y. Tong, H. Li, and H. Huang, Phys. Rev. Lett. **67**, 3102 (1991).
[14] J. J. Barton, Phys. Rev. Lett. **67**, 3106 (1991).
[15] M. Guizar-Sicairos and J. R. Fienup, J. Opt. Soc. Am. A **29**, 2367 (2012).
[16] C. Gaur, B. Mohan, and K. Khare, J. Opt. Soc. Am. A **32**, 1922 (2015).
[17] T. Latychevskaia and H.-W. Fink, Phys. Rev. Lett. **98**, 233901 (2007).
[18] C. Cho, B. Choi, H. Kang, and S. Lee, Opt. Express **20**, 22454 (2012).
[19] L. Rong, Y. Li, S. Liu, W. Xiao, F. Pan, and D. Wang, Opt. Lasers Eng. **51**, 553 (2013).
[20] B. D. Haeffele, S. Roth, L. Zhou, and R. Vidal, in *2017 IEEE 14th International Symposium on Biomedical Imaging* (IEEE, Melbourne, 2017), p. 741.
[21] Y. Rivenson, Y. Zhang, H. Günaydın, D. Teng, and A. Ozcan, Light Sci. Appl. **7**, 17141 (2018).
[22] D. L. Donoho, IEEE Trans. Inf. Theory **52**, 1289 (2006).
[23] L. Zhu, W. Zhang, D. Elnatan, and B. Huang, Nat. Methods **9**, 721 (2012).
[24] D. Gross, Y.-K. Liu, S. T. Flammia, S. Becker, and J. Eisert, Phys. Rev. Lett. **105**, 150401 (2010).
[25] A. Shabani, R. L. Kosut, M. Mohseni, H. Rabitz, M. A. Broome, M. P. Almeida, A. Fedrizzi, and A. G. White, Phys. Rev. Lett. **106**, 100401 (2011).
[26] W.-X. Wang, R. Yang, Y.-C. Lai, V. Kovanis, and C. Grebogi, Phys. Rev. Lett. **106**, 154101 (2011).
[27] G. A. Howland, J. Schneeloch, D. J. Lum, and J. C. Howell, Phys. Rev. Lett. **112**, 253602 (2014).
[28] D. J. Brady, K. Choi, D. L. Marks, R. Horisaki, and S. Lim, Opt. Express **17**, 13040 (2009).
[29] J. W. Goodman, *Introduction to Fourier Optics*, 3rd ed (Roberts and Company Publishers, Greenwood Village, 2005).
[30] See Supplemental Material at http://link.aps.org/supplemental/10.1103/PhysRevLett.121.093902 for formula derivation, explanation of terms and simulation results.
[31] E. J. Candes and M. B. Wakin, IEEE Signal Process. Mag. **25**, 21 (2008).
[32] L. I. Rudin, S. Osher, and E. Fatemi, Physica (Amsterdam) **60D**, 259 (1992).
[33] J. M. Bioucas-Dias and M. A. T. Figueiredo, IEEE Trans. Image Process. **16**, 2992 (2007).
[34] https://github.com/THUHoloLab/CS_twin_image_removal_1.
[35] M. Liebling and M. Unser, J. Opt. Soc. Am. A **21**, 2424 (2004).
[36] H. Zhang, L. Cao, H. Zhang, W. Zhang, G. Jin, and D. J. Brady, Opt. Express **25**, 24991 (2017).